Determination of stellar parameters for FGK-dwarf stars: the NIR approach

by

Daniel Thaagaard Andreasen

A thesis submitted in conformity with the requirements
for the degree of Doctor of Philosophy
Graduate Department of Departamento de Fisica e Astronomia
University of Porto

Dedication

To Linnea, Henriette, and Rico

For always supporting me

Acknowledgements

Lorem ipsum dolor sit amet, consectetuer adipiscing elit. Ut purus elit, vestibulum ut, placerat ac, adipiscing vitae, felis. Curabitur dictum gravida mauris. Nam arcu libero, nonummy eget, consectetuer id, vulputate a, magna. Donec vehicula augue eu neque. Pellentesque habitant morbi tristique senectus et netus et malesuada fames ac turpis egestas. Mauris ut leo. Cras viverra metus rhoncus sem. Nulla et lectus vestibulum urna fringilla ultrices. Phasellus eu tellus sit amet tortor gravida placerat. Integer sapien est, iaculis in, pretium quis, viverra ac, nunc. Praesent eget sem vel leo ultrices bibendum. Aenean faucibus. Morbi dolor nulla, malesuada eu, pulvinar at, mollis ac, nulla. Curabitur auctor semper nulla. Donec varius orci eget risus. Duis nibh mi, congue eu, accumsan eleifend, sagittis quis, diam. Duis eget orci sit amet orci dignissim rutrum.

Nam dui ligula, fringilla a, euismod sodales, sollicitudin vel, wisi. Morbi auctor lorem non justo. Nam lacus libero, pretium at, lobortis vitae, ultricies et, tellus. Donec aliquet, tortor sed accumsan bibendum, erat ligula aliquet magna, vitae ornare odio metus a mi. Morbi ac orci et nisl hendrerit mollis. Suspendisse ut massa. Cras nec ante. Pellentesque a nulla. Cum sociis natoque penatibus et magnis dis parturient montes, nascetur ridiculus mus. Aliquam tincidunt urna. Nulla ullamcorper vestibulum turpis. Pellentesque cursus luctus mauris.

Abstract

Nam dui ligula, fringilla a, euismod sodales, sollicitudin vel, wisi. Morbi auctor lorem non justo. Nam lacus libero, pretium at, lobortis vitae, ultricies et, tellus. Donec aliquet, tortor sed accumsan bibendum, erat ligula aliquet magna, vitae ornare odio metus a mi. Morbi ac orci et nisl hendrerit mollis. Suspendisse ut massa. Cras nec ante. Pellentesque a nulla. Cum sociis natoque penatibus et magnis dis parturient montes, nascetur ridiculus mus. Aliquam tincidunt urna. Nulla ullamcorper vestibulum turpis. Pellentesque cursus luctus mauris.

Resumo

Nam dui ligula, fringilla a, euismod sodales, sollicitudin vel, wisi. Morbi auctor lorem non justo. Nam lacus libero, pretium at, lobortis vitae, ultricies et, tellus. Donec aliquet, tortor sed accumsan bibendum, erat ligula aliquet magna, vitae ornare odio metus a mi. Morbi ac orci et nisl hendrerit mollis. Suspendisse ut massa. Cras nec ante. Pellentesque a nulla. Cum sociis natoque penatibus et magnis dis parturient montes, nascetur ridiculus mus. Aliquam tincidunt urna. Nulla ullamcorper vestibulum turpis. Pellentesque cursus luctus mauris.

Contents

List of Tables

List of Figures

Chapter 4

Results for FGK stars

> Don't cry because it's over, smile because it happened.
>
> Dr. Seuss

It is time to apply the theory and methodology on some data. In this chapter results from studies during the thesis will be presented. There is the analysis of three stars which lead to two papers, HD20010 (Andreasen et al., 2016) and Arcturus & 10 Leo (Andreasen et al., 2017a). Additionally, there was an analysis of how a cut in excitation potential might affect the final parameters of a star. This will be discussed in Section 4.6, and last the analysis of a range of synthetic spectra from the PHOENIX spectral library (Husser et al., 2013), with $T_{\rm eff}$ lower than analysed in previous stars with the methodology described above in Section 3.3. However, before diving into the results of the analysis it is important to describe how the NIR line list were compiled and why and how it was later refined.

4.1 The creation of a NIR line list

As discussed extensively in Chapter 2 and Chapter 3, an atomic line list is needed for employing the method described here. This line list is made by neutral and ionized iron lines in the NIR. This has already been mentioned in Chapter 2. Here the process will be explained in greater detail below for the two versions presented in Andreasen et al. (2016) and Andreasen et al. (2017b), respectively.

4.1.1 First version

The first version of a NIR iron line list for determining stellar atmospheric parameters of high resolution and high S/N spectra were presented in Andreasen et al. (2016). Other NIR line lists exists such as the one from Lindgren et al. (2016); Önehag et al. (2012) for utilising the synthetic method described above. Here all iron transitions between 10 000 Å to 25 000 Å[1] were downloaded from the VALD database (Kupka et al., 2000; Piskunov et al., 1995). This only includes Fe I and Fe II transitions. In total were 50 198 Fe I and 28 339 Fe II lines respectively acquired.

Add more line lists from the literature.

The EW of all lines were measured in the solar atlas by Hinkle et al. (1995). The EWs were measured using `ARES` due to the large amount of lines and to be as consistent as possible in the measurements.

[1] That is equivalent to the YJHK bands.

Since ARES expect a 1D spectrum with equidistant wavelength step, the solar spectrum was interpolated onto a regular wavelength grid of 0.01 Å. This did not change the appearance, and hence not the EW, of the final spectrum. This wavelength step is equivalent to a spectral resolution of 1 500 000 at 15 000 Å.

The EWs were measured by fitting Gaussian profiles to the spectral lines. For a given line, ARES output the central wavelength of the line (provided in the line list), the FWHM maximum of the fitted line, the number of lines fitted for the final result (in case of blending), the depth of the line, the EW of the line, and the Gaussian coefficients of the line. In the latest version of ARES , the error of the EW is also provided (Sousa et al., 2015).

More lines were discarded according to the following four criteria:

- Lines with EW lower than 5 mÅ as these lines can be problematic to see in spectra with lower S/N or spectra with many spectral features. Therefore the measurements of these lines are less reliable than stronger lines.
- Lines with EW higher than 200 mÅ as these lines are too strong to be fitted with a Gaussian profile. These lines might also be saturated and do not contain information about the abundance (see Figure 2.5).
- Lines where the total number of fitted lines are 10 or higher since they show indications of severe blending.
- If the fitted central wavelength is more than 0.05 Å away from the wavelength provided by VALD3 to avoid false identification. This should also remove some blended lines.

After this removal the number of Fe I and Fe II lines are reduced to 6060 and 2735, respectively.

4.1.1.1 Visual removal of lines

At this point a visual inspection were necessary. All absorption lines from all elements were downloaded from the VALD3 database in a 3 Å window around each of the nearly 9000 iron lines from the previous step. For each small spectral window, all absorption lines (including the iron line(s)) were plotted on top of the solar spectrum. An iron line were discarded if another line had the same central wavelength and/or the absorption line were severely blended. Most of the discarded iron lines had high EP, which are weak compared to the low EP lines. Therefore, it is fair to assume that many of these iron lines were falsely identified as another stronger line from another element. After the visual removal the number of Fe I and Fe II lines were reduced to a mere 593 and 22, respectively.

For some of the absorption lines it was not clear which element was the cause. These lines were marked for further investigation with synthesis as described below.

4.1.1.2 Synthetic investigation

For the lines marked above for further investigation an even broader window were used of 6 Å. Once again, all lines were downloaded from the VALD3 database in these spectral windows. MOOG were used with the *synth* driver to create a synthetic spectrum using a solar atmosphere model with $T_{\rm eff} = 5777$ K, $\log g = 4.438$, $A(\mathrm{Fe}) = 7.47$, and $\xi_{\rm micro} = 1.00$ km/s. The iron abundance (7.47) is from Gonzalez and Laws (2000). The overall metallicity for the solar atmosphere model is $[\mathrm{M/H}] = 0.00$ by definition. This was done for all spectral windows for three different $[\mathrm{Fe/H}] = \{-0.2, 0.0, 0.2\}$. Before creating a

synthetic spectrum all elements which are more than singly ionised were removed since MOOG does not allow these. An example of this can be seen in Figure 4.1. Here the neutral iron line at 15 550.439 Å were investigated. The three coloured curves are synthetic spectra with the three different [Fe /H]. Note that while [Fe /H] is used as a proxy for the over metallicity, [M /H], it is here specific only the iron abundance that is changed. The upper plot shows the result with the full VALD3 line list, while in the lower plot the iron line were removed from the line list. In this case it is clear that the iron line is the cause of the absorption line. The grey curve is the solar atlas for reference.

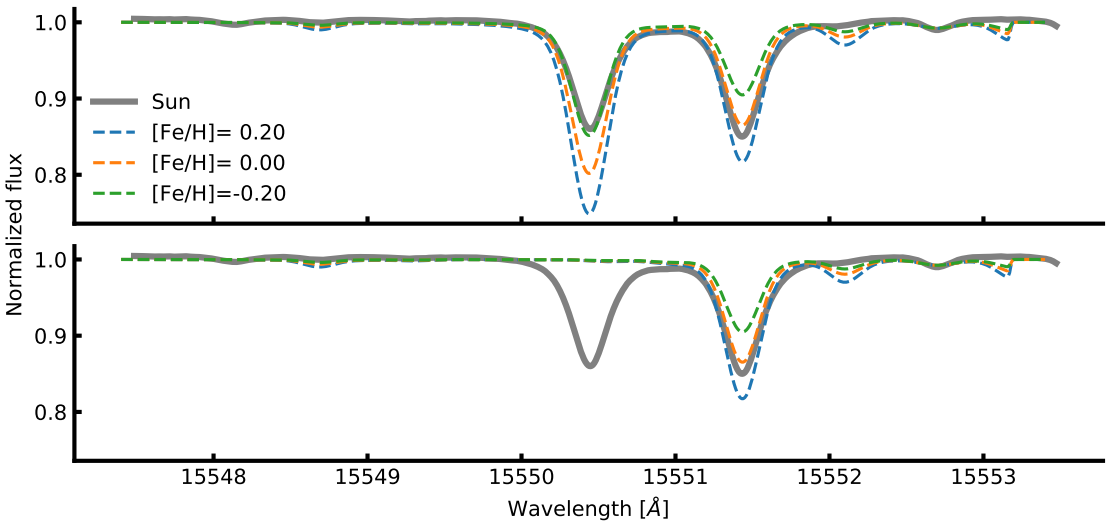

Figure 4.1: The three coloured curves represents different iron abundance, $\{-0.2, 0.0, 0.2\}$ dex compared to solar abundance. The grey curve is the solar atlas for reference. In this case the iron line at 15 550.439 Å is investigated. *Upper* plot: Synthetic spectra were computed using the full VALD line list in the spectral range for the three different iron abundances. *Lower* plot: Same as the upper plot, but with the iron line removed from the line list. Since the synthetic spectra shows no features at this absorption line anymore, it is a fair assumption to say the iron line is the cause of this absorption line.

If the three synthetic spectra shows variation at the iron line of interest, then it is assumed that the iron line is the cause for the absorption line. As a simple test, the iron line was also removed from the line list used to create the synthetic spectra. If the iron line in the synthetic spectra disappeared, it was a clear signal that this line can be used in the final iron line list (this can be seen clearly in the lower plot of Figure 4.1). In some cases two iron lines had the same or very similar wavelength, and this technique was used to include the right iron line. In cases where both iron lines causes the absorption line, they were both discarded since they are blended.

In a few cases two iron lines had the same wavelength and EP but different $\log gf$. If these both cause an iron line they can be combined into a single line by adding their gf values. After this step, there was 414 Fe I lines and 12 Fe II lines, respectively.

4.1.1.3 Calibrating the line list: astrophysical $\log gf$ values

These lines were collected into a single line list in the format required by MOOG (Sneden, 1973) and the line abundance were measured by all lines using the solar atmosphere model described above. If the

derived abundance for a single line differs by more than 1.0 dex from the solar iron abundance, the line would be discarded. The solar iron abundance used is 7.47 as found by Gonzalez and Laws (2000).

Why do we remove above 1.0dex?

After the removal of the lines mentioned above, the final line list is almost compiled. At this point the line list has to be calibrated. This is done by changing $\log gf$ so the line abundance for all iron lines are 7.47 when using the solar atmosphere model mentioned above. As mentioned in Section 2.3 there is a anti-correlation between the abundance of a line and $\log gf$. This means a bisector minimization can be used to locate the $\log gf$ that gives the desired abundance.

This was done for all the iron lines at this stage. It is important to calibrate a line list if the setup of parameter determination is changed somehow. This includes the type of model atmospheres used (e.g. ATLAS9 or MARCS), the interpolation code to generate a model atmosphere from the grid, or the settings of the radiative code, here `MOOG` .

4.1.1.4 Removal of high dispersion lines

The line list calibrated above was used to derive parameters for HD 20010 (see Section 4.2), however the derived parameters showed poor results when compared to the literature values. This lead to the following test, where highly disperse lines would be removed.

A Gaussian distribution was made for the EW of each line centred on the EW itself,

$$f(x, EW, \sigma) = \frac{1}{\sqrt{2\pi\sigma^2}} e^{-\frac{(x-EW)^2}{2\sigma^2}}, \tag{4.1}$$

where σ is the error on the EW, expressed by Cayrel (1988):

$$\sigma \simeq 1.6 \frac{\sqrt{\Delta\lambda EW}}{S/N}, \tag{4.2}$$

where $\Delta\lambda = 0.1$ and a S/N=50 is considered here, which is much lower than the actual S/N of the solar atlas. 100 draws of the distribution above were made for each line and derive the abundance using the solar atmosphere model. The mean absolute deviation (MAD) were calculated for each line abundance. The MAD for each line as a function of the original measured EW can be seen in Figure 4.2. The trend for the weaker lines is expected since a small absolute change in the EW results in a large relative change in abundance. However, this does not mean these lines have a high dispersion. Therefore the disperse lines are found in the de-trended MAD value, where an exponential function is used for de-trending. A single point above 3σ is removed iteratively in the de-trended data. After this process there are 334 Fe I lines and 13 Fe II lines.

4.1.2 Second version

As will be seen in Section 4.2.1 the line list presented above were used to derive atmospheric parameters of HD 20010. Even though the first test of the line list was success-full, it left room for improvements. The errors on the derived parameters were quite high for the spectral type compared results obtainable with a similar analysis utilising the optical spectrum (see Section 4.2.1 for details on this). Additionally, the derived metallicity was 0.10 dex higher than the literature values used.

Make sure to actually discuss this!

If all derived parameters except metallicity are reliable (when compared to e.g. a literature value), then it suggest that the measured EW are either over- or underestimated. However, when using a line

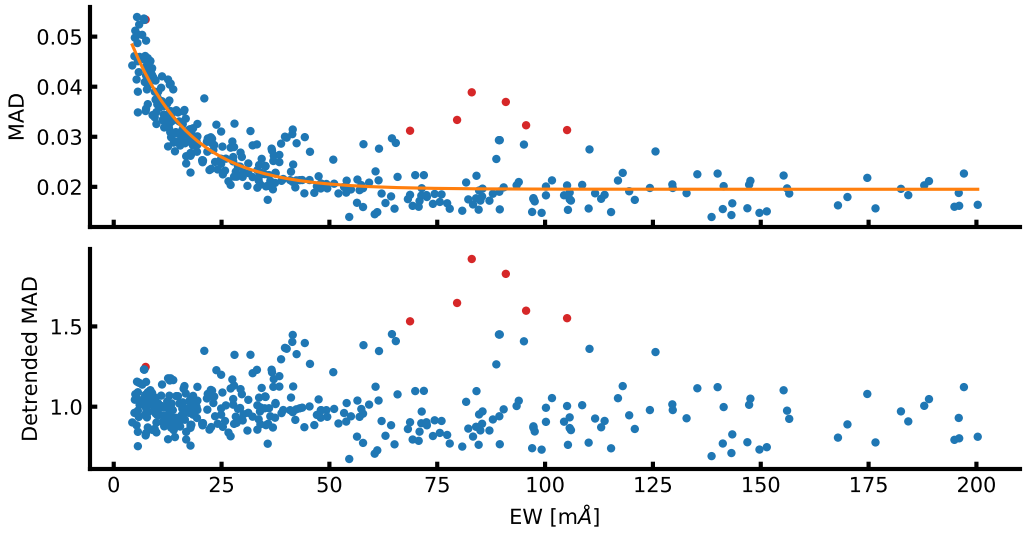

Figure 4.2: The most disperse lines. *Upper* plot: The MAD versus the original EW. The red points are the outliers which were discarded during this process. *Lower* plot: Same as above with the MAD being de-trended by the exponential fit as shown in the upper panel.

list for the first time like here, it can also suggest problems with the line list itself, for example a bad calibration. This could have been wrong measurements of the EWs of the calibrator star, Sun in this case. This combines to several cases:

- Correct measurement of EW of calibrator star:
  - Systematic lower measurement of EW of target star leads to underestimated [M /H]
  - Systematic higher measurement of EW of target star leads to overestimated [M /H]
  - Correct measurement of EW of target star leads to correct [M /H]
- Systematic lower measurements of EW of calibrator star:
  - Systematic lower measurement of EW of target star leads to underestimated [M /H]
  - Systematic higher measurement of EW of target star can lead to correct or overestimated [M /H]
  - Correct measurement of EW of target star leads to underestimated [M /H]
- Systematic higher measurements of EW of calibrator star:
  - Systematic lower measurement of EW of target star can lead to correct or underestimated [M /H]
  - Systematic higher measurement of EW of target star leads to overestimated [M /H]
  - Correct measurement of EW of target star leads to overestimated [M /H]

It is important to note, that *correct* has been used here, assuming a perfect setup, that includes perfect model atmosphere, perfect radiative transfer code, etc. In reality the final [M/H] (and the other parameters) measured by different group will occasionally differ regarding the setup used.

As described in Section 4.1.1 the EW of the Sun (calibrator star) was measured with `ARES` . A crucial option to set when using `ARES` is the `rejt` parameter as mentioned in Section 3.3.2. This option is used to place the continuum and will this directly affect the measured EW. At the time of compiling the first version of the line list it seems the `rejt` value used did not reflect the high S/N of the spectrum, thus placing the continuum too low and thereby underestimate the EW.

In this second version of the line list, the goal is to:

1. Make sure the EW measurements are as correct as possible by measuring them by hand
2. Free of blended lines in cooler stars (K stars in this case)

The second point is a similar exercise which was done in the optical by Tsantaki et al. (2013), where blended lines were removed from the larger line list by Sousa et al. (2008). This allowed to determine the atmospheric parameters of stars colder than 5000 K. However, the optical spectrum still suffer for severely blended lines at low $T_{\rm eff}$, thus this method does not work for M stars.

Both of the above steps were done at the same time, by measuring the EWs by hand using `IRAF`. Whenever a line was difficult to reliably measure, i.e. a consistent measurement was not possible/easy, it was discarded since it was blended. This can be seen in ...where the EW measurements from the first version is shown against this version with the manual measurements.

Make a plot with EW before and after

Continue from here

4.2 HD20010

HD 20010 is a star that has been analysed twice with the methodology described here in this thesis. First time this star was analysed was in Andreasen et al. (2016) when the NIR line list was published. Later this line list was revised leading to a removal of several lines. This resulted in the second analysis in Andreasen et al. (2017a); both described below.

4.2.1 First analysis

To test our new line list we search for a well-studied solar-type star. The spectrum for such a target needs to be available in the NIR at both high resolution and high S/N. An ideal place to look for such a star is the CRIRES-POP database (Lebzelter et al., 2012b). Here, the best target for testing is HD 20010, an F8 subgiant star. This star has been part of many surveys and is therefore well studied. Different parameters from the literature are listed in Table 3. The data available at CRIRES-POP are in the raw format and pipeline reduced, while three small pieces of the spectra are fully reduced on the web page 3 . The data is in the standard CRIRES format with each fits file including four binary tables with the data from the four detectors. In the future, the final reduced data will be presented by the CRIRES-POP team. In contrast to the pipeline reduced data, this will be of higher quality, a better wavelength calibration, and telluric correction. We measured the EWs of the pipeline reduced spectra, and where there was an overlap with the fully reduced spectrum, we measured both as a consistency check. The measured EWs from the fully reduced spectra were consistent with the measured EWs from the pipeline reduced spectra. As mentioned above, we use the Y, J, H, and K-bands which are all available for this star. The

spectra come in pieces of 50 Å to 120 Å. These pieces over- lap each other, and we were able to measure the EW for a single line up to five times. Unfortunately, wavelength calibration is a difficult task for CRIRES owing to the rather small spectral regions measured on each detector. Each calibration was performed separately for each detector and required the avail- ability of a sufficient number of calibration lines in the respective spectral region. This was not always the case and a default linear solution was applied. A pipeline reduced spectrum shows up as a stretched spectrum if the wavelength calibration is poor compared to a model spectrum or a solar spectrum, for example. The wavelength calibration does not have any effect on the signal-to-noise ratio, which is generally high for the spectrum of HD 20010. The signal-to-noise varies between 200 and 400 for different chunks. The pipeline reduced spectra for HD 20010 contains tellurics and the wavelength is shifted in radial velocity. All of these factors make the line identification very difficult, and so we developed a program to properly identify the lines, which does the following:

1. Plotting the observed spectrum
2. Overplotting a model spectrum. In this particular case the solar spectrum was used since the atmospheric parameters are close enough, so the sun was able to serve as a model
3. Overplotting a telluric spectrum from the TAPAS web page (Bertaux et al., 2014)
4. Overplotting vertical lines at the location of lines in the list
5. Calculating the cross-correlation function (CCF) for the telluric spectrum with respect to the observed spectrum, locating the maximum value by a Gaussian fit, and using this to shift the telluric spectrum with the found RV;
6. Performing the same as step 5, but for the model
7. Shifting the lines with the same RV as found for the model/solar spectrum.

The final plot shows the shifted spectra, and the CCFs at the sides. An example of the software in use is shown in Fig. 6. The two RVs are part of the title of the plot. Once the lines were identified, the EWs were measured with the splot routine in Image Reduction and Analysis Facility (IRAF). The reason not to choose `ARES` for this task was to visually confirm the identification of the line given the relative poor wavelength calibration. We were able to measure 249 Fe I lines and 5 Fe II lines compared to 344 Fe I lines and 13 Fe II lines for the Sun over the whole NIR spectral region. Whenever we had more than one measurement of a line, the average was used for the final EW. We derived the stellar parameters using the standard procedure (see Sect. 2.6) as done for the Sun. Given the relatively low quality of the spectrum of HD 20010 (see below) and be- cause it is not corrected for telluric contamination, we made a cut in EW at 5 mÅ in order to remove the lines which are most affected by contamination from either telluric or other line blends. Additionally, we made a cut in EP at 5.5 eV because the Fe I and Fe II lines usually used for stellar parameter determination in the optical regime are also limited to similar values (see e.g Sousa et al., 2008). Higher excitation potential lines are also more likely to be affected by non-LTE effects. When deriving the atmospheric parameters, we made a 3σ outlier removal in the abundance iteratively until there were no more outliers present. Since we could only measure 5 Fe II lines, for comparison we also decided to derive parameters using the same method, but we fixed the surface gravity to the reference value. The resulting atmospheric parameters and iron abundances are presented

in Table 4. The effective temperature, surface gravity, and metallicity agree within the errors with the literature values. Similar parameters are obtained by fixing log g to the average literature value or by leaving it free.

The errors on the atmospheric parameters for HD 20010 are much higher than what is achievable with other measurements in the literature, as presented above in Table 3. In order to explain these errors, we calculated the abundances for all lines which have at least two measurements of the EW. We then calculated the abundances for the highest measured EW and the lowest. The differences in abundances are presented in Fig. 7. The very large differences (more than 0.1 dex) translate to the high errors in the parameters.

The source of the large errors on the parameters can be seen more clearly where abundances are compared to excitation potential or abundances versus reduced EW. Here the dispersion on the abundances can be seen clearly, as shown in Fig. 8.

This test strongly suggest that errors in the EWs, likely due to the poor quality of this spectrum, are responsible for the relatively large error bars in the derived stellar parameters. Systematic errors (e.g. due to a possible non-optimal reduction of the spectrum) may be the reason for these large error bars. As the CRIRES-POP team continue their great efforts in reducing the optimal spectra, it will be interesting to re-visit this star once the entire spectrum has been fully reduced.

4.2.2 Second analysis

As a first step we revisit HD 20010 for which we derived atmospheric stellar parameters in Paper I using the newly revised line list presented in this paper. The results are shown in Table 4.1 along with the results for the two other stars analysed in this work. We see better agreement with the average literature values adopted (especially [Fe /H] and $\log g$), and smaller errors with the updated results. This suggests that the new line list is more reliable.

Table 4.1: Results for the three stars with first set of parameters are the set of parameters are results with $\log g$ set to the same value during the minimization procedure as found in the literature (fixed), and last set of parameters are with all parameters free during the minimization procedure.

	HD 20010	10 Leo	Arcturus
Literature			
$T_{\rm eff}$ (lit.)	6152 ± 95	4741 ± 60	4300 ± 110
$\log g$ (lit.)	3.96 ± 0.19	2.76 ± 0.17	1.60 ± 0.29
[Fe /H] (lit.)	-0.27 ± 0.06	-0.03 ± 0.02	-0.54 ± 0.11
$\xi_{\rm micro}$ (lit.)	1.17 ± 0.24	1.45 ± 0.08	1.93 ± 0.13
$\log g$ fixed			
$T_{\rm eff}$	6161 ± 164	4761 ± 118	4357 ± 74
$\log g$	3.96 (fixed)	2.76 (fixed)	1.60 (fixed)
[Fe /H]	-0.18 ± 0.11	0.01 ± 0.07	-0.55 ± 0.04
$\xi_{\rm micro}$	1.72 ± 0.44	1.25 ± 0.11	1.55 ± 0.10
All free			
$T_{\rm eff}$	6162 ± 184	4805 ± 98	4439 ± 62
$\log g$	4.08 ± 0.77	2.42 ± 0.61	1.20 ± 0.20
[Fe /H]	-0.18 ± 0.11	-0.01 ± 0.07	-0.58 ± 0.06
$\xi_{\rm micro}$	1.59 ± 0.49	1.23 ± 0.10	1.55 ± 0.10

The parameters for the three stars, omitting the Sun since the derived parameters are trivial with a

calibrated line list[2], are presented in Fig. 4.3. We show the literature values (blue), derived parameters with $\log g$ fixed to the literature value (green), and derived parameters when $\log g$ is free during the minimization procedure (red points).

4.3 Arcturus

Arcturus is one of the brightest stars on the night sky with a V magnitude of -0.05 (Ducati, 2002). Hence it is a prime target for testing with the numerous measurements of the atmospheric parameters as mentioned above.

The atlas consists of both a summer observation set and a winter observation set. The two data sets have been obtained in order to minimise the effect of tellurics at different spectral regions. A comparison between the two sets of measured EWs - both the manual measurements using IRAF and the measurements for the summer set and winter set show excellent agreement with a dispersion of 7 mÅ. This means that the two data sets are very similar, thus we decided to only manually measure the EWs for one set (summer). We did, however, measure a few lines from the winter data set to verify the agreement. Since the EWs are very similar we chose to only derive parameters of the summer set with EWs measured with `ARES` . Parameters were derived with and without $\log g$ set to a fixed value (1.60 dex, the average literature value adopted). The derivation of the parameters followed the procedure presented in Paper I, although we used the minimization routine of FASMA (Andreasen et al., 2017b). After we reached convergence using all the iron lines we were able to measure, one outlier above 3σ in abundance were removed, and the minimization routine was restarted. This process was done iteratively until there were no more outliers. The final results are presented in Table 4.1 together with mean parameters from the literature.

We generally see good agreement between the derived parameters and the average values from the literature adopted (see Table 4.1). The only parameter being difficult to measure is the surface gravity due to the low number of Fe II lines in the NIR. It is very important to derive the metallicity accurately, and we report consistent results overall.

4.4 10 Leo

The approach for determining the atmospheric stellar parameters for 10 Leo is identical to Arcturus. We use `ARES` on each band (YJ, H, and K-band) separately. For the small gaps in the spectrum, we simply set the flux to 1, since the spectrum is already normalised. This will also prevent `ARES` to identify and measure any lines in these regions. The EWs from the three regions are combined to one final line list used for the determination of the parameters. The final results can be seen in Fig. 4.3 and Table 4.1.

Generally the derived parameters are in excellent agreement with the literature values listed here. For $T_{\rm eff}$ we were 64 K off with $\log g$ set as a free parameter, well within the errors. The only parameter that show a discrepancy compared to the literature value is $\xi_{\rm micro}$ with a difference of 0.22 km/s, which is at the limit of the errors reported. We note that this parameter is not reported in the PASTEL database, and this was a derived parameter from a empirical relation. We were able to derive good $\log g$ values, although with larger errors compared to the results from the literature.

[2] The solar parameters used were: $T_{\rm eff} = 5777$ K, $\log g = 4.44$ dex, [Fe /H] = 0.00 dex, and $\xi_{\rm micro} = 1.00$ km/s.

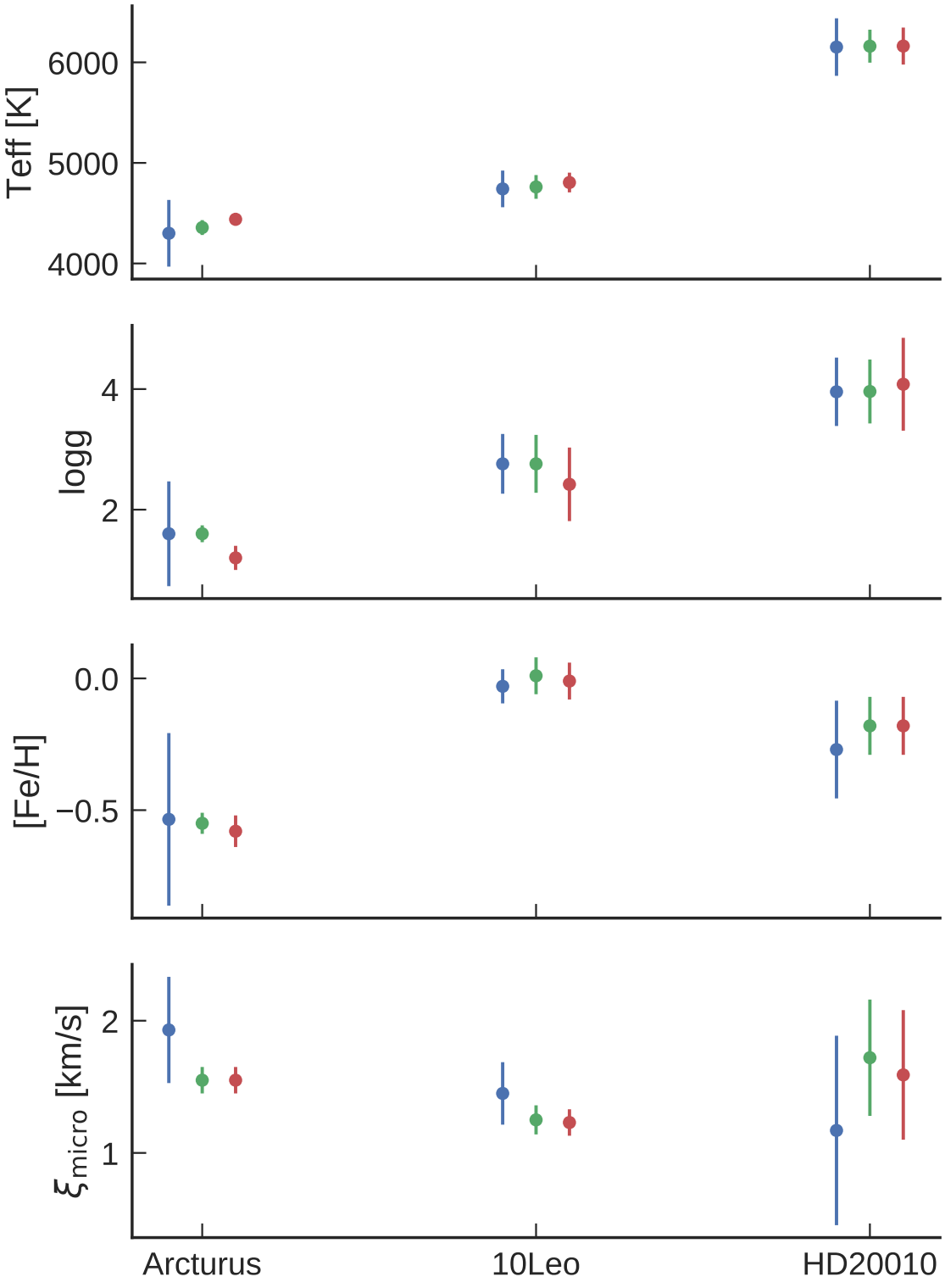

Figure 4.3: Parameters for Arcturus, 10 Leo, and HD 20010 (revisited in this paper). The blue points show the literature values from the PASTEL database as discussed in the text. The green points are the derived values with $\log g$ fixed to the literature value, and the red points show the derived parameters when $\log g$ is also derived.

4.5 Synthetic cool stars

4.6 Parameter dependence on EP cut

It is common practise, as in this case, to make a cut in EP for a line list when deriving parameters. This was suggested in Andreasen et al. (2016) (later done in Andreasen et al., 2017a) for the NIR line list used here. This cut was made at 5.5 eV, inspired by a similar cut in the optical (Sousa et al., 2008), including only lines below this limit. The lines with higher EP might also be affected by non-LTE effects which is not treated in this methodology.

As the parameters are dependent on this cut in EP, it seemed interesting to divide a line list in two with upper and lower EPs and analyse those separately. Before going into that analysis it is important to note, that the parameters should not depend on any cut in EP if the theory is right, the radiative transfer code is working properly, and the atmospheric models are correct. Lines with different EP are likely to be formed in different layers of the atmosphere as discussed in Section 2.2, however this should not effect the final derived abundance, which is the problem here.

Make a figure that shows this

Bibliography

Adibekyan, V. Z., Benamati, L., Santos, N. C., Alves, S., Lovis, C., Udry, S., Israelian, G., Sousa, S. G., Tsantaki, M., Mortier, A., Sozzetti, A., and De Medeiros, J. R.: 2015, *MNRAS* **4**50, 1900

Aerts, C., Christensen-Dalsgaard, J., and Kurtz, D. W.: 2010, *Asteroseismology*, Springer-Verlag

Ammler-von Eiff, M., Santos, N. C., Sousa, S. G., Fernandes, J., Guillot, T., Israelian, G., Mayor, M., and Melo, C.: 2009, *A&A* **5**07, 523

Andreasen, D. T., Sousa, S. G., Delgado Mena, E., Santos, N. C., Lebzelter, T., Mucciarelli, A., and Neil, J. J.: 2017a, *A&A* **5**85, A143

Andreasen, D. T., Sousa, S. G., Delgado Mena, E., Santos, N. C., Tsantaki, M., Rojas-Ayala, B., and Neves, V.: 2016, *A&A* **5**85, A143

Andreasen, D. T., Sousa, S. G., Tsantaki, M., Teixeira, G. D. C., Mortier, A., Santos, N. C., Suárez-Andrés, L., Delgado Mena, E., and Ferreira, A. C. S.: 2017b, *A&A* **6**00, A69

Artigau, É., Kouach, D., Donati, J.-F., Doyon, R., Delfosse, X., Baratchart, S., Lacombe, M., Moutou, C., Rabou, P., Parès, L. P., Micheau, Y., Thibault, S., Reshetov, V. A., Dubois, B., Hernandez, O., Vallée, P., Wang, S.-Y., Dolon, F., Pepe, F. A., Bouchy, F., Striebig, N., Hénault, F., Loop, D., Saddlemyer, L., Barrick, G., Vermeulen, T., Dupieux, M., Hébrard, G., Boisse, I., Martioli, E., Alencar, S. H. P., do Nascimento, J.-D., and Figueira, P.: 2014, in *Society of Photo-Optical Instrumentation Engineers (SPIE) Conference Series*, Vol. 9147 of *Society of Photo-Optical Instrumentation Engineers (SPIE) Conference Series*, p. 15

Baraffe, I., Homeier, D., Allard, F., and Chabrier, G.: 2015, *A&A* **5**77, A42

Bedding, T. R., Mosser, B., Huber, D., Montalbán, J., Beck, P., Christensen-Dalsgaard, J., Elsworth, Y. P., García, R. A., Miglio, A., Stello, D., White, T. R., De Ridder, J., Hekker, S., Aerts, C., Barban, C., Belkacem, K., Broomhall, A.-M., Brown, T. M., Buzasi, D. L., Carrier, F., Chaplin, W. J., di Mauro, M. P., Dupret, M.-A., Frandsen, S., Gilliland, R. L., Goupil, M.-J., Jenkins, J. M., Kallinger, T., Kawaler, S., Kjeldsen, H., Mathur, S., Noels, A., Silva Aguirre, V., and Ventura, P.: 2011, *Nature* **4**71, 608

Bensby, T., Feltzing, S., and Oey, M. S.: 2014, *A&A* **5**62, A71

Bertaux, J. L., Lallement, R., Ferron, S., Boonne, C., and Bodichon, R.: 2014, *A&A* **5**64, A46

Blackwell, D. E. and Shallis, M. J.: 1977, *MNRAS* **1**80, 177

Bochanski, J. J., Hawley, S. L., Covey, K. R., West, A. A., Reid, I. N., Golimowski, D. A., and Ivezić, Ž.: 2010, *AJ* **1**39, 2679

Boyajian, T. S., von Braun, K., van Belle, G., McAlister, H. A., ten Brummelaar, T. A., Kane, S. R., Muirhead, P. S., Jones, J., White, R., Schaefer, G., Ciardi, D., Henry, T., López-Morales, M., Ridgway, S., Gies, D., Jao, W.-C., Rojas-Ayala, B., Parks, J. R., Sturmann, L., Sturmann, J., Turner, N. H., Farrington, C., Goldfinger, P. J., and Berger, D. H.: 2012, *ApJ* **7**57, 112

Casagrande, L., Portinari, L., and Flynn, C.: 2006, *MNRAS* **3**73, 13

Casagrande, L., Ramírez, I., Meléndez, J., Bessell, M., and Asplund, M.: 2010, *A&A* **5**12, A54

Cayrel, R.: 1988, in G. Cayrel de Strobel and M. Spite (eds.), *The Impact of Very High S/N Spectroscopy on Stellar Physics*, Vol. 132 of *IAU Symposium*, p. 345

Chaplin, W. J., Kjeldsen, H., Christensen-Dalsgaard, J., Basu, S., Miglio, A., Appourchaux, T., Bedding, T. R., Elsworth, Y., García, R. A., Gilliland, R. L., Girardi, L., Houdek, G., Karoff, C., Kawaler, S. D., Metcalfe, T. S., Molenda-Żakowicz, J., Monteiro, M. J. P. F. G., Thompson, M. J., Verner, G. A., Ballot, J., Bonanno, A., Brandão, I. M., Broomhall, A.-M., Bruntt, H., Campante, T. L., Corsaro, E., Creevey, O. L., Doğan, G., Esch, L., Gai, N., Gaulme, P., Hale, S. J., Handberg, R., Hekker, S., Huber, D., Jiménez, A., Mathur, S., Mazumdar, A., Mosser, B., New, R., Pinsonneault, M. H., Pricopi, D., Quirion, P.-O., Régulo, C., Salabert, D., Serenelli, A. M., Silva Aguirre, V., Sousa, S. G., Stello, D., Stevens, I. R., Suran, M. D., Uytterhoeven, K., White, T. R., Borucki, W. J., Brown, T. M., Jenkins, J. M., Kinemuchi, K., Van Cleve, J., and Klaus, T. C.: 2011, *Science* **3**32, 213

Christensen-Dalsgaard, J., Kjeldsen, H., Brown, T. M., Gilliland, R. L., Arentoft, T., Frandsen, S., Quirion, P.-O., Borucki, W. J., Koch, D., and Jenkins, J. M.: 2010, *ApJL* **7**13, L164

Conod, U., Blind, N., Wildi, F., and Pepe, F.: 2016, in *Society of Photo-Optical Instrumentation Engineers (SPIE) Conference Series*, Vol. 9909 of *Proceedings of the SPIE*, p. 990941

Czekala, I., Andrews, S. M., Mandel, K. S., Hogg, D. W., and Green, G. M.: 2015, *ApJ* **8**12, 128

Delfosse, X., Donati, J.-F., Kouach, D., Hébrard, G., Doyon, R., Artigau, E., Bouchy, F., Boisse, I., Brun, A. S., Hennebelle, P., Widemann, T., Bouvier, J., Bonfils, X., Morin, J., Moutou, C., Pepe, F., Udry, S., do Nascimento, J.-D., Alencar, S. H. P., Castilho, B. V., Martioli, E., Wang, S. Y., Figueira, P., and Santos, N. C.: 2013, in L. Cambresy, F. Martins, E. Nuss, and A. Palacios (eds.), *SF2A-2013: Proceedings of the Annual meeting of the French Society of Astronomy and Astrophysics*, pp 497–508

Dotter, A., Chaboyer, B., Jevremović, D., Kostov, V., Baron, E., and Ferguson, J. W.: 2008, *ApJS* **1**78, 89

Ducati, J. R.: 2002, *VizieR Online Data Catalog* 2237

Follert, R., Dorn, R. J., Oliva, E., Lizon, J. L., Hatzes, A., Piskunov, N., Reiners, A., Seemann, U., Stempels, E., Heiter, U., Marquart, T., Lockhart, M., Anglada-Escude, G., Löwinger, T., Baade, D., Grunhut, J., Bristow, P., Klein, B., Jung, Y., Ives, D. J., Kerber, F., Pozna, E., Paufique, J., Kaeufl, H. U., Origlia, L., Valenti, E., Gojak, D., Hilker, M., Pasquini, L., Smette, A., and Smoker, J.: 2014, in *Society of Photo-Optical Instrumentation Engineers (SPIE) Conference Series*, Vol. 9147 of *Society of Photo-Optical Instrumentation Engineers (SPIE) Conference Series*, p. 19

Girardi, L., Bressan, A., Bertelli, G., and Chiosi, C.: 2000, *A&A Supp.* **1**41, 371

Gonzalez, G. and Laws, C.: 2000, *AJ* **1**19, 390

Gray, D. F.: 2005, *The Observation and Analysis of Stellar Photospheres, 3rd ed.*

Grundahl, F., Fredslund Andersen, M., Christensen-Dalsgaard, J., Antoci, V., Kjeldsen, H., Handberg, R., Houdek, G., Bedding, T. R., Pallé, P. L., Jessen-Hansen, J., Silva Aguirre, V., White, T. R., Frandsen, S., Albrecht, S., Andersen, M. I., Arentoft, T., Brogaard, K., Chaplin, W. J., Harpsøe, K., Jørgensen, U. G., Karovicova, I., Karoff, C., Kjærgaard Rasmussen, P., Lund, M. N., Sloth Lundkvist, M., Skottfelt, J., Norup Sørensen, A., Tronsgaard, R., and Weiss, E.: 2017, *ApJ* **8**36, 142

Gustafsson, B., Edvardsson, B., Eriksson, K., Jørgensen, U. G., Nordlund, Å., and Plez, B.: 2008, *A&A* **4**86, 951

Hinkle, K. H., Wallace, L., and Livingston, W.: 1995, in A. J. Sauval, R. Blomme, and N. Grevesse (eds.), *Laboratory and Astronomical High Resolution Spectra*, Vol. 81 of *Astronomical Society of the Pacific Conference Series*, p. 66

Huber, D., Silva Aguirre, V., Matthews, J. M., Pinsonneault, M. H., Gaidos, E., García, R. A., Hekker, S., Mathur, S., Mosser, B., Torres, G., Bastien, F. A., Basu, S., Bedding, T. R., Chaplin, W. J., Demory, B.-O., Fleming, S. W., Guo, Z., Mann, A. W., Rowe, J. F., Serenelli, A. M., Smith, M. A., and Stello, D.: 2014, *ApJS* **2**11, 2

Husser, T.-O., Wende-von Berg, S., Dreizler, S., Homeier, D., Reiners, A., Barman, T., and Hauschildt, P. H.: 2013, *A&A* **5**53, A6

Kippenhahn, R. and Weigert, A.: 1994, *Stellar Structure and Evolution*, Springer-Verlag

Kjeldsen, H. and Bedding, T. R.: 1995, *A&A* **2**93, 87

Kotani, T., Tamura, M., Suto, H., Nishikawa, J., Sato, B., Aoki, W., Usuda, T., Kurokawa, T., Kashiwagi, K., Nishiyama, S., Ikeda, Y., Hall, D. B., Hodapp, K. W., Hashimoto, J., Morino, J.-I., Okuyama, Y., Tanaka, Y., Suzuki, S., Inoue, S., Kwon, J., Suenaga, T., Oh, D., Baba, H., Narita, N., Kokubo, E., Hayano, Y., Izumiura, H., Kambe, E., Kudo, T., Kusakabe, N., Ikoma, M., Hori, Y., Omiya, M., Genda, H., Fukui, A., Fujii, Y., Guyon, O., Harakawa, H., Hayashi, M., Hidai, M., Hirano, T., Kuzuhara, M., Machida, M., Matsuo, T., Nagata, T., Onuki, H., Ogihara, M., Takami, H., Takato, N., Takahashi, Y. H., Tachinami, C., Terada, H., Kawahara, H., and Yamamuro, T.: 2014, in *Society of Photo-Optical Instrumentation Engineers (SPIE) Conference Series*, Vol. 9147 of *Society of Photo-Optical Instrumentation Engineers (SPIE) Conference Series*, p. 14

Kupka, F. G., Ryabchikova, T. A., Piskunov, N. E., Stempels, H. C., and Weiss, W. W.: 2000, *Baltic Astronomy* **9**, 590

Kurucz, R.: 1993, *ATLAS9 Stellar Atmosphere Programs and 2 km/s grid. Kurucz CD-ROM No. 13. Cambridge, Mass.: Smithsonian Astrophysical Observatory, 1993.* 13

Lebzelter, T., Heiter, U., Abia, C., Eriksson, K., Ireland, M., Neilson, H., Nowotny, W., Maldonado, J., Merle, T., Peterson, R., Plez, B., Short, C. I., Wahlgren, G. M., Worley, C., Aringer, B., Bladh, S., de Laverny, P., Goswami, A., Mora, A., Norris, R. P., Recio-Blanco, A., Scholz, M., Thévenin, F., Tsuji, T., Kordopatis, G., Montesinos, B., and Wing, R. F.: 2012a, *A&A* **5**47, A108

Lebzelter, T., Seifahrt, A., Uttenthaler, S., Ramsay, S., Hartman, H., Nieva, M.-F., Przybilla, N., Smette, A., Wahlgren, G. M., Wolff, B., Hussain, G. A. J., Käufl, H. U., and Seemann, U.: 2012b, *A&A* **5**39, A109

Lindgren, S., Heiter, U., and Seifahrt, A.: 2016, *A&A* **5**86, A100

Meléndez, J. and Barbuy, B.: 1999, *ApJS* **1**24, 527

Mucciarelli, A., Pancino, E., Lovisi, L., Ferraro, F. R., and Lapenna, E.: 2013, *ApJ* **7**66, 78

Neuforge-Verheecke, C. and Magain, P.: 1997, *A&A* **3**28, 261

Önehag, A., Heiter, U., Gustafsson, B., Piskunov, N., Plez, B., and Reiners, A.: 2012, *A&A* **5**42, A33

Origlia, L., Oliva, E., Baffa, C., Falcini, G., Giani, E., Massi, F., Montegriffo, P., Sanna, N., Scuderi, S., Sozzi, M., Tozzi, A., Carleo, I., Gratton, R., Ghinassi, F., and Lodi, M.: 2014, in *Society of Photo-Optical Instrumentation Engineers (SPIE) Conference Series*, Vol. 9147 of *Society of Photo-Optical Instrumentation Engineers (SPIE) Conference Series*, p. 1

Piskunov, N. E., Kupka, F., Ryabchikova, T. A., Weiss, W. W., and Jeffery, C. S.: 1995, *A&A Supp.* **1**12, 525

Quirrenbach, A., Amado, P. J., Caballero, J. A., Mundt, R., Reiners, A., Ribas, I., Seifert, W., Abril, M., Aceituno, J., Alonso-Floriano, F. J., Ammler-von Eiff, M., Antona Jiménez, R., Anwand-Heerwart, H., Azzaro, M., Bauer, F., Barrado, D., Becerril, S., Béjar, V. J. S., Benítez, D., Berdiñas, Z. M., Cárdenas, M. C., Casal, E., Claret, A., Colomé, J., Cortés-Contreras, M., Czesla, S., Doellinger, M., Dreizler, S., Feiz, C., Fernández, M., Galadí, D., Gálvez-Ortiz, M. C., García-Piquer, A., García-Vargas, M. L., Garrido, R., Gesa, L., Gómez Galera, V., González Álvarez, E., González Hernández, J. I., Grözinger, U., Guàrdia, J., Guenther, E. W., de Guindos, E., Gutiérrez-Soto, J., Hagen, H.-J., Hatzes, A. P., Hauschildt, P. H., Helmling, J., Henning, T., Hermann, D., Hernández Castaño, L., Herrero, E., Hidalgo, D., Holgado, G., Huber, A., Huber, K. F., Jeffers, S., Joergens, V., de Juan, E., Kehr, M., Klein, R., Kürster, M., Lamert, A., Lalitha, S., Laun, W., Lemke, U., Lenzen, R., López del Fresno, M., López Martí, B., López-Santiago, J., Mall, U., Mandel, H., Martín, E. L., Martín-Ruiz, S., Martínez-Rodríguez, H., Marvin, C. J., Mathar, R. J., Mirabet, E., Montes, D., Morales Muñoz, R., Moya, A., Naranjo, V., Ofir, A., Oreiro, R., Pallé, E., Panduro, J., Passegger, V.-M., Pérez-Calpena, A., Pérez Medialdea, D., Perger, M., Pluto, M., Ramón, A., Rebolo, R., Redondo, P., Reffert, S., Reinhardt, S., Rhode, P., Rix, H.-W., Rodler, F., Rodríguez, E., Rodríguez-López, C., Rodríguez-Pérez, E., Rohloff, R.-R., Rosich, A., Sánchez-Blanco, E., Sánchez Carrasco, M. A., Sanz-Forcada, J., Sarmiento, L. F., Schäfer, S., Schiller, J., Schmidt, C., Schmitt, J. H. M. M., Solano, E., Stahl, O., Storz, C., Stürmer, J., Suárez, J. C., Ulbrich, R. G., Veredas, G., Wagner, K., Winkler, J., Zapatero Osorio, M. R., Zechmeister, M., Abellán de Paco, F. J., Anglada-Escudé, G., del Burgo, C., Klutsch, A., Lizon, J. L., López-Morales, M., Morales, J. C., Perryman, M. A. C., Tulloch, S. M., and Xu, W.: 2014, in *Society of Photo-Optical Instrumentation Engineers (SPIE) Conference Series*, Vol. 9147 of *Society of Photo-Optical Instrumentation Engineers (SPIE) Conference Series*, p. 1

Ramírez, I. and Meléndez, J.: 2005a, *ApJ* **6**26, 446

Ramírez, I. and Meléndez, J.: 2005b, *ApJ* **6**26, 465

Rayner, J., Bond, T., Bonnet, M., Jaffe, D., Muller, G., and Tokunaga, A.: 2012, in *Ground-based and Airborne Instrumentation for Astronomy IV*, Vol. 8446 of *Proceedings of the SPIE*, p. 84462C

Rayner, J., Tokunaga, A., Jaffe, D., Bonnet, M., Ching, G., Connelley, M., Kokubun, D., Lockhart, C., and Warmbier, E.: 2016, in *Society of Photo-Optical Instrumentation Engineers (SPIE) Conference Series*, Vol. 9908 of *Proceedings of the SPIE*, p. 990884

Recio-Blanco, A., Bijaoui, A., and de Laverny, P.: 2006, *MNRAS* **3**70, 141

Santos, N. C., Sousa, S. G., Mortier, A., Neves, V., Adibekyan, V., Tsantaki, M., Delgado Mena, E., Bonfils, X., Israelian, G., Mayor, M., and Udry, S.: 2013, *A&A* **5**56, A150

Sneden, C. A.: 1973, *Ph.D. thesis*, THE UNIVERSITY OF TEXAS AT AUSTIN.

Sousa, S. G., Santos, N. C., Adibekyan, V., Delgado-Mena, E., and Israelian, G.: 2015, *A&A* **5**77, A67

Sousa, S. G., Santos, N. C., Israelian, G., Mayor, M., and Monteiro, M. J. P. F. G.: 2007, *A&A* **4**69, 783

Sousa, S. G., Santos, N. C., Mayor, M., Udry, S., Casagrande, L., Israelian, G., Pepe, F., Queloz, D., and Monteiro, M. J. P. F. G.: 2008, *A&A* **4**87, 373

Torres, G., Andersen, J., and Giménez, A.: 2010, *Astronomy and Astrophysics Reviews* **1**8, 67

Torres, G., Fischer, D. A., Sozzetti, A., Buchhave, L. A., Winn, J. N., Holman, M. J., and Carter, J. A.: 2012, *ApJ* **7**57, 161

Torres, G., Winn, J. N., and Holman, M. J.: 2008, *ApJ* **6**77, 1324

Tsantaki, M., Andreasen, D. T., Teixeira, G. D. C., Sousa, S. G., Santos, N. C., Delgado-Mena, E., and Bruzual, G.: 2017, *MNRAS* **5**55, A150

Tsantaki, M., Sousa, S. G., Adibekyan, V. Z., Santos, N. C., Mortier, A., and Israelian, G.: 2013, *A&A* **5**55, A150

Tsantaki, M., Sousa, S. G., Santos, N. C., Montalto, M., Delgado-Mena, E., Mortier, A., Adibekyan, V., and Israelian, G.: 2014, *A&A* **5**70, A80

Valenti, J. A. and Fischer, D. A.: 2005, *ApJS* **1**59, 141

Valenti, J. A. and Piskunov, N.: 1996, *A&A Supp.* **1**18, 595